



Adsorption and sequestration of cadmium ions by polyptychial mesoporous biochar derived from *Bacillus* sp. biomass

Feng Li^{1,2} · Yixin Tang^{1,2} · Chengcheng Li^{1,2} · Yang Zheng^{1,2} · Xingwang Liu^{1,2} · Chuang Feng^{1,2} · Wan Zhao^{1,2} · Fang Wang^{1,2}

Received: 5 March 2019 / Accepted: 28 May 2019 / Published online: 14 June 2019
© Springer-Verlag GmbH Germany, part of Springer Nature 2019

Abstract

Bacteria-derived biochars from *Bacillus* sp. biomass under different pyrolysis temperature (250 °C, 350 °C, 450 °C, and 550 °C, respectively) were prepared, forming polyptychial, mesoporous graphite-like structure. The adsorption and sequestration efficiencies of Cd²⁺ by these biochars were evaluated, and the underlying mechanisms were then discussed. Cd²⁺ sorption data could be well described by Langmuir mode while the pseudo-second-order kinetic model and Elovich model best fitted the kinetic data. The functional groups complexation, cation- π interactions, and interaction with minerals (including surface precipitation with phosphorus and ion exchange) jointly contributed to Cd²⁺ sorption and sequestration on biochar, but the interaction with minerals played a dominant role by forming insoluble cadmium salt composed by polycrystalline and/or amorphous phosphate-bridged ternary complex. The maximum sorption capacity of BBC350 in simulated water phase of soil for Cd²⁺ was 34.6 mg/g. Furthermore, the addition of bacteria-derived biochars (1%, w/w) decreased the fractions easily absorbed by plants for Cd in the test paddy soils by 1.9–26% in a 10-day time. Results of this study suggest that bacteria-derived biochar would be a promising functional material in environmental and agricultural application.

Keywords Heavy metals · Bacterial biochar · Sorption · Sequestration · Soil remediation · Polyptychial structure

Introduction

Soils contaminated with heavy metals (HMs) could have adverse implications for food quality and safety and have attracted much public concern especially after the frightening media reports of cadmium (Cd) in Hunan-grown rice in China in 2013 (Yu 2016). Based on a 9-year survey of contaminants in soils from 2005 to 2013 conducted by China's Ministry of Environmental Protection (MEP) and Ministry of Land and Resources (MLR),

19.4% agricultural soils surveyed was classified as being contaminated, of which HM contamination accounts for the majority (82.4%) (MEP 2016). Notably among the HMs, Cd ranks the first in the percentage of 7.0% soil samples exceeding the MEP limit (MEP 2016). A substantial amount of Cd in agricultural soil is bioavailable to crops, and the bioavailability was highly influenced by Cd mobility.

Sequestration of soil Cd would be a potential remedial strategy for reducing the health and environmental risk. Indeed, current remedial actions of HM-contaminated soil recur to two strategies (Liu et al. 2018a): (i) ex situ extracting and/or separating HMs from soil including flotation and washing, with good remediation efficiency but high costs, and (ii) in situ stabilization of HMs including passivation, immobilization, and bio-mineralization, and are widely applied due to easy operation, low cost, and reliable remediation efficiency (Li et al. 2018). Recently, HM stabilization has been attracting domestic and international researchers' concerns in the field of soil remediation. Many stabilization sorbents have been studied to immobilize Cd in soil, including activated carbon, organic material, microbial biomass, and agricultural waste materials, but most of the sorbents have limitations of either low efficiency, re-release of HMs after

Responsible editor: Tito Roberto Cadaval Jr

Electronic supplementary material The online version of this article (<https://doi.org/10.1007/s11356-019-05610-3>) contains supplementary material, which is available to authorized users.

✉ Feng Li
lifeng6220@xtu.edu.cn

¹ College of Environment Science and Resources, Xiangtan University, Xiangtan 411105, People's Republic of China

² Hunan Engineering Laboratory for high efficiency purification technology and its application on complex heavy metal wastewater treatment, Xiangtan 411105, People's Republic of China

stabilization, or disposal restrictions (Peng et al. 2009; Liu et al. 2018a). To solve this issue, a high efficiency and environment-friendly sorbents with strong passivation capacities for HM ions are urgently needed.

Biochar is C-rich residue of incomplete combustion of biomass under oxygen-limited conditions at relatively low temperatures (< 700 °C). It is a promising soil conditioner for agricultural and environmental field because of its high surface area, porosity, sufficient functional groups, and easy accessibility, which distinguishes it from other carbonaceous products such as activated C (AC) and charcoal (Ahmad et al. 2014). Furthermore, application of biochar to soil can also help improve soil properties and enhance soil quality by retaining higher moisture, elevating nutrients, and microbial activity, therefore increasing crop yields (O'Connor et al. 2018; Yu et al. 2018).

The underlying mechanisms for Cd immobilization on biochar included (i) metal-ligand complexation; (ii) metal ion exchange with Cd^{2+} ; (iii) interaction between Cd^{2+} and π electrons (e.g., C=C, C=O); (iv) co-precipitation with mineral groups (e.g., PO_4^{3-} , CO_3^{2-}) (Zhang et al. 2015; Qiao et al. 2018; Xiao et al. 2018). The above mechanisms were enslaved by the components in raw materials (e.g., hemicellulose, cellulose, and lignin in plant-derived feedstocks) and pyrolysis temperature (Yang et al. 2007). In case of raw materials, bacterial biomass materials are good precursors because of their natural polyptychial spacial structure such as peptidoglycan layer. Peptidoglycan layer is a three-dimension network stereostructure and composed by linear glycan strands cross-linked by short peptides (Matias and Beveridge 2005). Thus, the polyptychial mesoporous graphite-like structure would probably occur in biochar derived by bacteria biomass, which would be expected to promote Cd immobilization. In addition, phosphorus in bacterial can be transformed from organic phosphorus to inorganic phosphorus during carbonization process. The transformation might also strengthen Cd sequestration by the elevated sorption sites for Cd^{2+} (Zhao et al. 2016). Interestingly, microcrystalline graphitic sheets (disordered graphene layers) within biochar stacked together and the graphitic sheets grew with increasing carbonization temperature beyond 600 °C. Consequently, the formation of graphitic sheets within biochar increased the π /cation- π interactions and thereby improved sorption of heavy metals on biochar (Harvey et al. 2011; Klupfel et al. 2014).

In order to evaluate the impacts of the morphology and structure of bacteria-derived biochars on adsorption and sequestration of Cd^{2+} , this study thus investigated the adsorption isotherms (such as Langmuir model and Freundlich model) and adsorption kinetics (including pseudo-first-order model, pseudo-second-order model, and Elovich model) of Cd^{2+} using biochars derived from *Bacillus* sp. biomass by the different pyrolysis temperature (250 °C, 350 °C, 450 °C, and 550 °C, respectively). Sequestration effectiveness was also

assessed by determining the leaching ratio based on the pH values of soil in the range from 5.0 to 6.0. Mechanisms responsible for Cd sequestration were illuminated using field emission scanning electron microscopy (SEM), transmission electron microscopy (TEM), energy dispersive X-ray analysis (EDX), select area electron diffraction (SAED), TEM mapping, and X-ray photoelectron spectroscopy (XPS). The results of this study would be expected to deepen the comprehension and broaden insights of the sequestration behavior of Cd in soils in the future remediation soils contaminated by HMs.

Materials and methods

Chemicals and materials

$3\text{CdSO}_4 \cdot 8\text{H}_2\text{O}$ (ultrapure grade) and other inorganic reagents (analytical grade) were purchased from Sinopharm Chemical Reagent Co., Ltd., Shanghai. Ultrapure water was used for all the experiments. Soils were collected from the top layer (0–20 cm) of the paddy soil located in Yangji village, Xiangtan, China. The content of Cd in collected paddy soil was 0.7 mg/kg and soil pH was 6.3, which was significantly higher than the Chinese environmental quality standard for agricultural soils (GB 15618–2018, 0.4 mg/kg at 5.5 < pH < 6.5).

Biochar preparation

Gram-positive bacterial cells of *Bacillus* sp. were cultivated in LB medium at 30 °C for 36 h before centrifugation (4000 rpm for 15 min) and were subsequently freeze-dried (LGJ-10, Henan Brother Equipment Co., Ltd., China). The powdered biomass was tightly placed in a ceramic pot, and then pyrolyzed in a tube furnace (OTF-1200X, HF-Kejing, China) under N_2 atmosphere (200 mL/min, 0.025 MPa), the pyrolysis was programmed to raise the internal biomass chamber temperature to the desired temperatures (250, 350, 450, and 550 °C, respectively) at a rate of 10 °C/min for 2 h (Luo et al. 2018). The bacteria-derived biochars were denoted as BBC250, BBC350, BBC450, and BBC550 in accordance with the desired pyrolysis temperature. All the biochar samples were ground to pass through a 0.25-mm sieve prior to use.

Bacteria-derived biochar characterizations

The special surface area and pore size distribution of bacteria-derived biochars (including BBC250, BBC350, BBC450, and BBC550) were analyzed by a NOVA-2200e Surface Area and Pore Size analyzer (Quantachrome, Boynton Beach, Florida, USA), respectively. After degassification under vacuum for 9 h at 150 °C, nitrogen absorption-desorption isotherms of the above bacteria-derived biochar samples were carried out.

The surface area was calculated with the Brunauer-Ebammatt-Teller (BET) method based on nitrogen sorption data in the relative pressure (P/P_0) range of 0 to 1. Pore volume and pore diameter were determined using the Barret-Joyner-Halender (BJH) method based on N_2 adsorption data. The total pore volume was obtained from the amount of nitrogen absorbed at a relative pressure (P/P_0) of 0.98 approximately. The pore size distribution was analyzed by a nonlocal density functional theory method using the data of nitrogen adsorption, which was assumed a slit pore model (Yuan et al. 2018).

To evaluate influences of pyrolysis temperature on the bacteria-derived biochar structure ordering, Raman spectra measurements were carried out on a Renishaw InVia Raman microscope (inVia, Renishaw, UK) with the excitation laser wavelength of 532 nm at room temperature (Liu et al. 2014).

Morphology and microstructure characteristics of bacteria-derived biochars before and after the adsorption of Cd^{2+} were observed using field emission scanning electron microscopy (SEM, JSM-6610LV, JEOL, Japan) at an accelerating voltage of 30 kV and transmission electron microscopy (TEM, Tecnai G2F30, FEI, USA) coupled with an energy dispersive X-ray system (EDX) at an acceleration voltage of 300 kV. High-resolution transmission electron microscopy (HRTEM) equipped with the select area electron diffraction (SAED) and TEM mapping were further used to investigate the potential crystal structure and distribution of adsorbed Cd^{2+} on bacteria-derived biochar (Yoo et al. 2018).

The surface chemical compositions of bacteria-derived biochar before and after the adsorption of Cd^{2+} (here referring to the bonding energies of Cd, P, O, and C) were determined using X-ray photoelectron spectroscopy (XPS, Escalab 250xi, Thermo Scientific, USA) (Guo et al. 2017).

Sorption experiments

Cadmium stock solution (1000 mg/L) was prepared by dissolving $3CdSO_4 \cdot 8H_2O$ in 0.01 mol/L $NaNO_3$ solution that simulated soil water phase background electrolyte. All vessels and experimental apparatuses were strictly acid-cleaned before use so as to avert the residual of metal ions.

The adsorption kinetic experiments were performed as follows: 10 mg BBC250, BBC350, BBC450, and BBC550 samples were placed into 10-mL solution containing 25 mg/L Cd^{2+} in glass vials, respectively, and then, the above glass vials were placed in a shaker (150 rpm) at 25 °C. At certain sampling time interval (1, 2, 3, 5, 7, 9, 11, 24, and 48 h), 10-mL subsamples were taken and Cd concentrations after filtration with 0.22- μm filters (MCE, Green Union Science Instrument Co., Ltd., China) were measured by air-acetylene flame atomic absorption spectrometry (AAS, AA-6300C, Shimadzu Co. Ltd., Suzhou, China) equipped with an air-acetylene flame atomizer and a hollow cathode lamp (AS-1, Beijing, China).

The adsorption isotherm experiments were carried out as the same conditions described above. In brief, 10-mg BBC250, BBC350, BBC450, and BBC550 samples were added into 10-mL $NaNO_3$ solution with different Cd levels (10, 15, 20, 25, 50, 80, and 100 mg/L) in 20-mL glass vials with Teflon-lined screw caps, respectively. The above mixture was placed in a shaker under 150 rpm at 25 °C for 24 h. After equilibrium, BBC250, BBC350, BBC450, and BBC550 and liquid phases were separated by centrifugation (3000 rpm for 15 min) before filtering through 0.22- μm filters.

Adsorption model and kinetics analysis

The adsorption amount of Cd^{2+} on bacteria-derived biochar at the certain time t (q_t , mg/g) was calculated using Eq. 1 (Wang et al. 2018),

$$q_t = (C_0 - C_t) \times V/m \tag{1}$$

where q_t is the amounts of Cd^{2+} adsorbed onto the bacteria-derived biochar (mg/g), V is the volume of the solution (L), m is the amount of adsorbent (g), C_0 and C_t represent the concentration of Cd^{2+} at initial time and at time t , respectively (mg/L), bacteria-derived biochar was referred to BBC250, BBC350, BBC450, and BBC550, respectively.

The pseudo-first-order and pseudo-second-order models (Luo et al. 2018) were used to investigate the effects of contact time on Cd adsorption on the bacteria-derived biochar, and the correlation coefficient (R^2) was considered as an evaluation of the consistency between the experimental data and the models. The pseudo-first-order kinetic model (Eq. 2) is given as follows:

$$q_t = q_e(1 - \exp(-k_1 t)) \tag{2}$$

The pseudo-second-order kinetic model consists by all the steps of adsorption including adsorption, external film diffusion, and internal particle diffusion. The equation is defined as Eq. 3.

$$qt = qe \left(1 - \frac{1}{1 + q_e k_2 t} \right) \tag{3}$$

Elovich model is another common model to reveal the chemisorption process, which assumes that the adsorbate is adsorbed onto the solid surface without desorption, and the adsorption rate reduces with increasing contact time due to an increased surface (Chien and Clayton 1980). The equation is expressed as Eq. 4,

$$q_t = \frac{1}{\beta} \ln(1 + \alpha \beta t) \tag{4}$$

where q_e and q_t (mg/g) represent the content of adsorbed Cd at the equilibrium and at time t , respectively. k_1 (h^{-1}) and k_2

(g/(mg/h)) represent adsorption rate constants. α (mg/(g·min)) is the initial adsorption rate and β (g/mg) is the constant concerned with the surface coverage and the chemisorption activation energy.

To compare the adsorption capacity and intensity of Cd^{2+} onto bacteria-derived biochar, Langmuir and Freundlich models were employed by fitting the experimental data of the adsorption isotherm. The equations of the two models are shown below (Gao et al. 2019):

$$qe = \frac{K_L q_{\max} C_e}{1 + K_L C_e} \quad (\text{Langmuir model}) \quad (5)$$

$$qe = K_F C_e^{1/n} \quad (\text{Freundlich model}) \quad (6)$$

where q_e (mg/g) and C_e (mg/L) represent the adsorption amount and the equilibrium concentration of Cd, respectively. The K_L (L/mg) and q_{\max} (mg/g) express the Langmuir adsorption constant and the maximum adsorption amount, respectively. K_F and n express the uptake capacity and adsorption intensity, respectively.

Sequestration capacity of Cd^{2+} by bacteria-derived biochar

To estimate the sequestration capacity of bacteria-derived biochar for Cd^{2+} , BBC350 adsorbed Cd^{2+} was selected to carry out the leaching experiment. Briefly, Cd-loaded BBC350 (0.5 g) was placed in a 1000-mL flask containing 500-mL HNO_3 solution (0.1 mol/L) in a shaker under 150 rpm at 25 °C for 480 min. After that, the supernatant was filtered by a 0.22- μm filter after centrifugation (3000 rpm for 15 min). The concentration of Cd^{2+} in filtrate was analyzed by AAS.

The sequestration ratio (SR) for Cd^{2+} by BBC350 was calculated as the following formulae, Eq. 7 and Eq. 8.

$$\text{SR} = \frac{(C_0 - C_a) \times (1 - E_e)}{C_0} \times 100\% \quad (7)$$

where C_0 is the initial content of Cd^{2+} concentration (mg/L), C_a is the concentration of Cd^{2+} (mg/L) at the equilibrium time (24 h) during adsorption step in the section of 2.3, C_L is the leaching concentration of Cd^{2+} (mg/L) at the equilibrium time (240 min) during leaching step. E_e (%) is the equilibrium elution efficiency of leaching step represented the proportion of the elution amount during the desorption step occupied in the amount of adsorption amount in previous adsorption step, which is calculated by the below Eq. 8.

$$E_e = \frac{C_L}{C_0 - C_a} \times 100\% \quad (8)$$

Phosphorus release from bacteria-derived biochar

Phosphorus release from BBC250, BBC350, BBC450, and BBC550 was separately investigated through a batch leaching experiment (Zhao et al. 2016). Briefly, biochar was mixed with 0.01 mol/L NaNO_3 solution at a solid/liquid ratio of 1:1 (w/v) and then agitated at 25 °C for 72 h. At certain sampling time intervals (1, 2, 3, 5, 7, 11, 24, 48, and 72 h), the leachate was collected and filtered using a 0.22- μm filter. After that, the phosphorus concentrations in the leachate were determined by colorimetry using the molybdate/ascorbic acid method (Cao and Harris 2010).

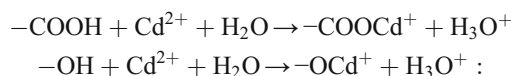
Quantitative analysis of sorption contribution ratio involved in different Cd^{2+} sorption mechanisms on bacteria-derived biochars

The sorption contributions of Cd^{2+} sorption on bacteria-derived biochars involving in the interaction and precipitation with minerals (Q_{\min}), functional group complexation (Q_{co}), and Cd^{2+} - π coordination ($Q_{\text{c}\pi}$) were analyzed as the methods described by Pal and Maiti (2019). Briefly, the surface minerals on bacteria-derived biochars were removed by soaking in 1 mol/L HCl solution overnight and then washed using pure water until to the neutral pH value. The reduced amount of Cd^{2+} from Cd-loaded bacteria-derived biochars by acidic soaking was considered as the contribution of these removed minerals, and the yield of demineralized biochars from initial bacteria-derived biochars was calculated to offset the concentration effect. The sorption involved in the interaction with minerals (Q_{\min}) was calculated by Eq. 9:

$$Q_{\min} = Q_t - Q_a * Y \quad (9)$$

where Q_{\min} (mg/g) is the amount of Cd^{2+} sorption attributed to the interaction with minerals, Q_t (mg/g) is the total sorption of Cd^{2+} on bacteria-derived biochars, Q_a (mg/g) is the amount of adsorbed Cd^{2+} on demineralized bacteria-derived biochars, Y is the yield of demineralized biochars from initial bacteria-derived biochars.

Additionally, in order to the coordination with the oxygen-containing organic groups on the surface of bacteria-derived biochars, a drop of 1 mol/L HCl solution was added to demineralized bacteria-derived biochars before and after Cd^{2+} sorption, where the chemical interaction below could exist:



Thus, the amount of H⁺ release could represent the contribution of functional group complexation (Q_{co}) to the adsorption of Cd²⁺. It could be calculated by Eq. 10:

$$Q_{co} = Q_{pH} * Y \tag{10}$$

where Q_{co} (mg/g) is the amount of Cd²⁺ sorption attributed to the functional groups complexation, Q_{pH} (mg/g) is the amount of adsorbed Cd²⁺ by functional groups complexation, Y is the yield of demineralized biochar from initial bacteria-derived biochars.

Cd²⁺ sorption on demineralized bacteria-derived biochars was the sum of Cd²⁺- π interaction and functional group complexation together, so the amount of Cd²⁺ sorption by Cd²⁺- π interaction ($Q_{c\pi}$) could be calculated by Eq. 11:

$$Q_{c\pi} = Q_a * Y - Q_{co} \tag{11}$$

Finally, the contribution ratios of Cd²⁺ sorption mechanisms involved in the interaction and precipitation with minerals, functional group complexation, and Cd²⁺- π coordination were calculated using the Q_{min}/Q_t , Q_{co}/Q_t , and $Q_{c\pi}/Q_t$, respectively.

Soil experiment

To verify the adsorption and sequestration capacity for Cd²⁺ in soil by bacteria-derived biochars, BBC250, BBC350, BBC450, and BBC550 were added as a ratio of 1% (w/w) to the tested paddy soils in pots under 70% soil moisture content for 10 days. No biochar addition was used as the control check (CK). Each treatment was triplicate. Soil samples were collected after 10 days and extracted continuously by 1.0 mol/L MgCl₂ at pH = 7 (exchangeable Cd) and 1.0 mol/L sodium acetate at pH = 5 (carbonate-bound Cd) (Tessier et al. 1979). The sum of exchangeable Cd and carbonate-bound Cd was considered to be the fractions easily absorbed by plants (FEA) for Cd in the tested soils, and FEA-Cd could be used to predict the bioavailabilities of heavy metals in soils and correlate with plant uptake (Walker et al. 2003).

Cadmium determination

Before measurement, samples were immediately acidified to pH < 2 with concentrated HNO₃. Cd²⁺ concentrations were measured by AAS. The calibration curve of Cd²⁺ was calculated by serial gradient solutions of Cd²⁺ in the range from 0.025 to 1.0 mg/L. The detection limit of Cd²⁺ was 0.00337 mg/L, and the relative standard deviation (RSD) was 0.2% (n = 6). FEA-Cd contents in the tested paddy soils were determined with ICP-MS (iCAP Qc, Thermo Scientific, USA). The instrumental calibration, data acquisition, and data analysis were controlled by the instrument software with the detection limit of 0.0006 μ g/L. The standard solutions of 0,

5.0, 10.0, 20.0, 40.0, and 50 μ g/L were used for instrumental calibration. The correlation coefficient in standard curve was > 0.999. Each test was replicated three times.

Statistical analysis

One-way analysis of variance (ANOVA) was used to assess significant differences at $p \leq 0.05$ among groups (Origin 8.5). All of the experiments were performed in triplicate and the data are presented as mean \pm standard deviation (SD).

Results and discussion

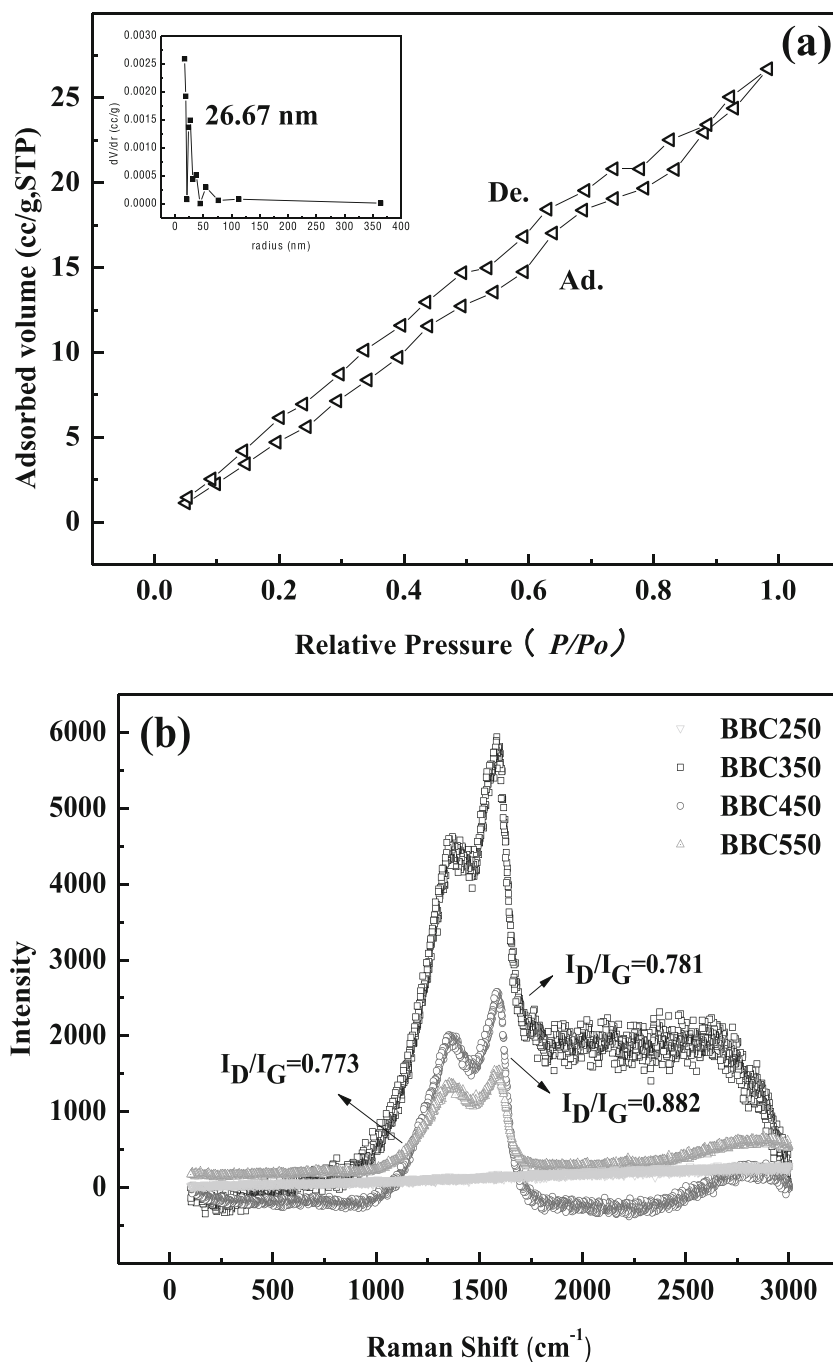
Properties of bacteria-derived biochar

The surface area and total pore volume of biochar are significant parameters related to adsorption efficiency for heavy metal ions, which influences amounts of binding sites (O'Connor et al. 2018). The surface areas of BBC250, BBC350, BBC450, and BBC550 were 24.0 m²/g, 65.2 m²/g, 38.2 m²/g, and 4.7 m²/g, respectively. Nitrogen sorption analysis showed that BBC250, BBC350, BBC450, and BBC550 presented the type IV isotherm characteristics of mesoporous material, and their narrow pore width distribution centered at 53.61 nm, 53.34 nm, 62.66 nm, and 46.81 nm, respectively (Fig. 1a and Table S1).

Raman spectra of BBC350, BBC450, and BBC550 showed that two important Raman peaks 1355 cm⁻¹ (D-band) induced by sp³ hybridization and 1573 cm⁻¹ (G-band) originated from crystalline graphitic/sp² carbon atoms, respectively (Fig. 1b), suggesting the appearance of graphitic-like structure in biochar (Mendonca et al. 2017). The intensity ratio of the D and G bands (I_D/I_G) indicates the graphitization degree and density of defects for carbon materials (Jiang et al. 2016). Here, the I_D/I_G increased from 0.781 to 0.882 with an increased pyrolytic temperature from 350 to 550 °C, elucidating that newly formed sp²-hybridized domains were dominant with higher defects, and preserved six or more fused hexatomic rings (suggesting the presence of aromatic or graphitic structures). The G peaks of bacteria-derived biochars were broadened significantly with the increased pyrolytic temperature from 350 to 550 °C, for instance, the G peaks of BBC550 from 1466.8 to 1746.9 cm⁻¹. This result could be related to the formation of graphitic and/or aromatic rings structures in biochar during the process of pyrolysis from 350 to 550 °C (Abdul et al. 2017).

The microstructures of BBC250, BBC350, BBC450, and BBC550 were presented by SEM and TEM images (Fig. 2 and Fig. S1). BBC250 and BBC350 showed typically rough and porous natures, while BBC450 and BBC550

Fig. 1 **a** N_2 adsorption-desorption isotherms of BBC350, **b** Raman spectra of BBC 250, BBC350, BBC450, and BBC550

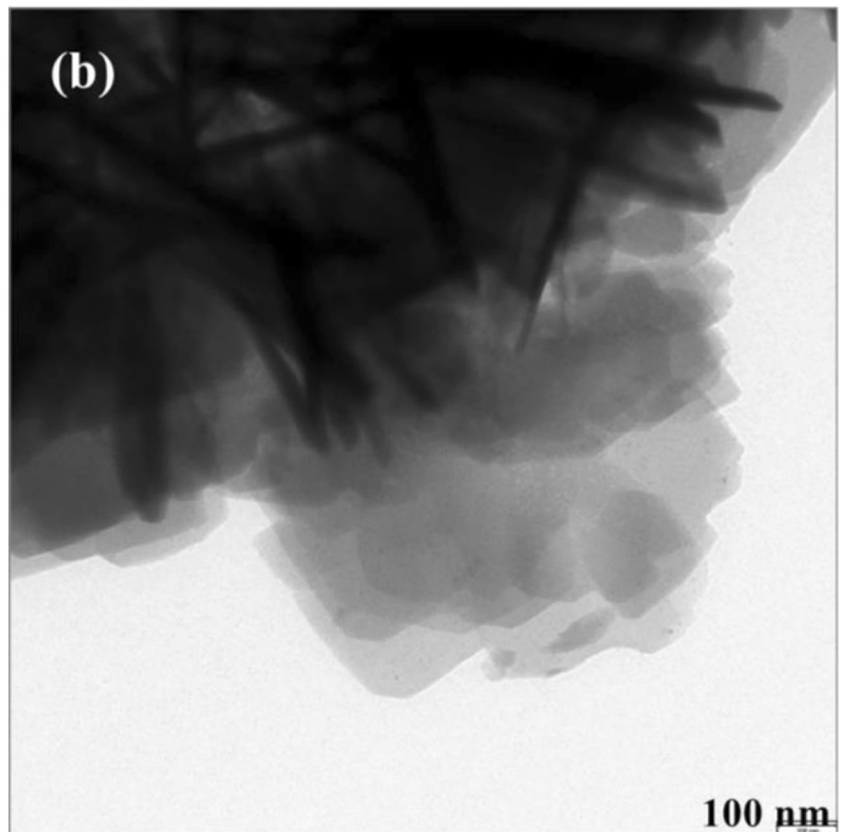
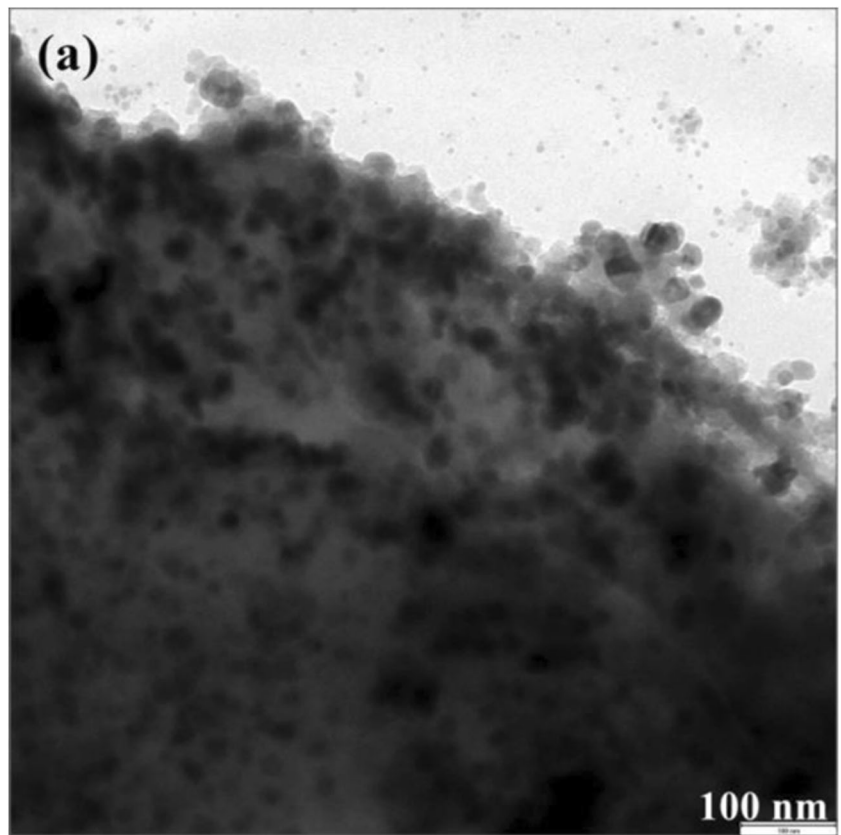


clearly appeared polyptychial structures and visible pores, which convincingly supported the results of Raman spectra (Fig. 1b). Also, the TEM observations of BBC350 and BBC550 were similar with the membrane structure of graphene oxide (Chen et al. 2017). Overall, these results shown in Table S1, Figs. 1 and 2 show that these biochars had mesoporous, polyptychial, and graphene-like structure, which suggested a greater potential for bacteria-derived biochar to sequester Cd^{2+} compared to simple pore structure of other biochars.

Adsorption isotherms and kinetics of Cd^{2+} on bacteria-derived biochar

The adsorption kinetics of Cd^{2+} on BBC250, BBC350, BBC450, and BBC550 including the pseudo-first-order, pseudo-second-order, and Elovich models are shown in Fig. 2 while the kinetics fitting parameters for the adsorption of Cd^{2+} onto BBC250, BBC350, BBC450, and BBC550 are listed in Table S2. As shown in Fig. 2a and Table S2, the pseudo-second-order model better fitted the adsorption of

Fig. 2 TEM images of Cd^{2+} before (a) and after (b) adsorption onto BBC350, SEM images of Cd^{2+} before (c) and after (d) adsorption onto BBC550



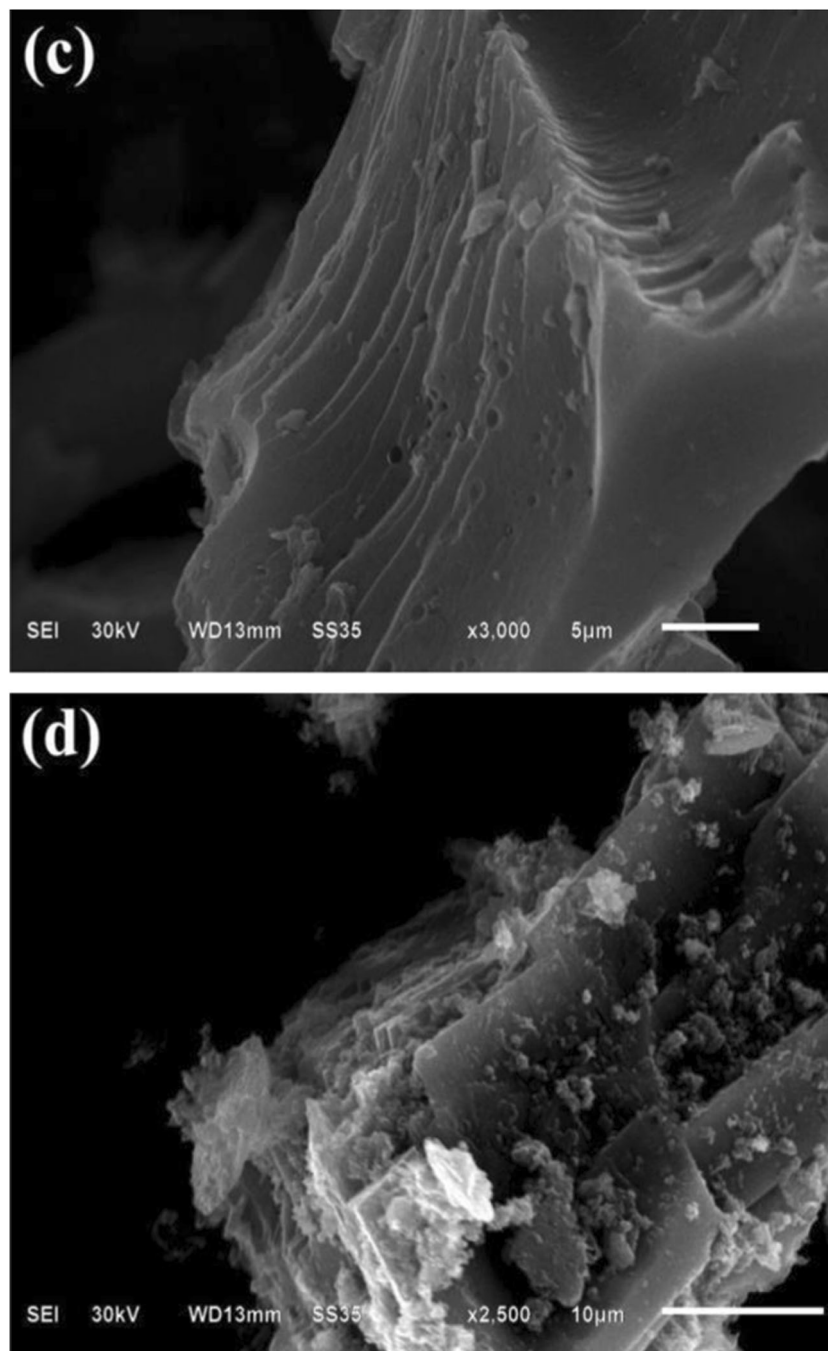


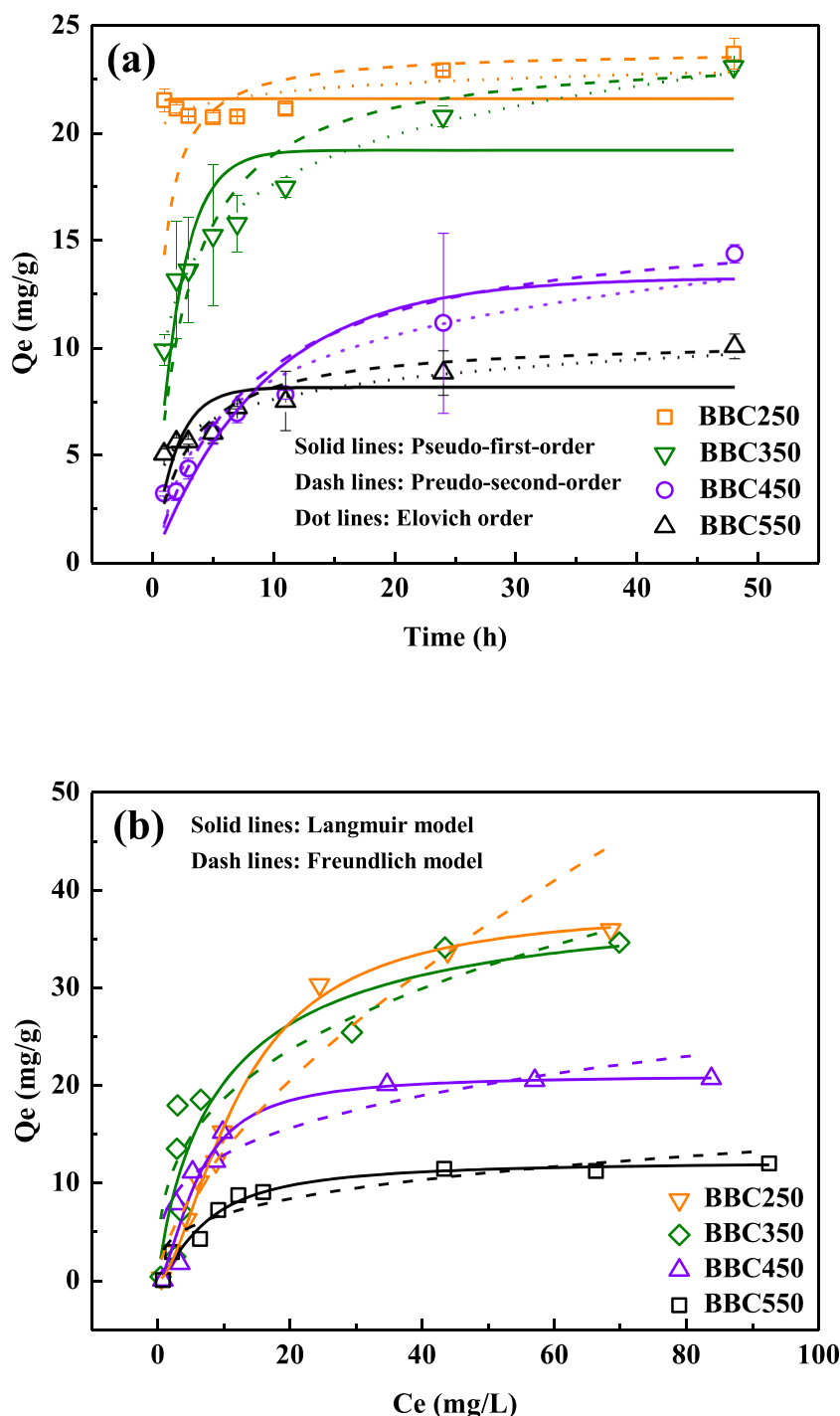
Fig. 2 (continued)

Cd^{2+} on bacteria-derived biochar as suggested by their higher correlation coefficients (R^2) than that of pseudo-first-order model. This indicated that the adsorption of Cd^{2+} on bacteria-derived biochar was dominated by chemisorption mechanism (Guo et al. 2017). Furthermore, the correlation coefficient of Elovich model was higher than 0.90 except for that of BBC250, which also suggested that chemical interactions played an important role during the adsorption process of Cd^{2+} onto bacteria-derived biochar (Deng et al. 2019). Additionally, hexagon graphitic sheets occurred within

BBC350, BBC450, and BBC550 (Fig. 1b), which could induce cation- π interaction, and thereby increase the adsorption of Cd^{2+} on bacteria-derived biochars. This result was consistent with the findings of Harvey et al. (2011), where they confirmed that cation- π bonding mechanisms play a crucial role in the sorption of HM ions on biochars.

As shown in SEM images (Figs. 2 and S1), bacteria-derived biochars have more homogeneous surface and more obvious multilayered structure with the increase of pyrolytic temperature, which was against the initial cadmium sorption

Fig. 3 **a** Adsorption kinetics of Cd^{2+} on BBC250, BBC350, BBC450, and BBC550 at 298 K, **b** adsorption isotherm for adsorption of Cd^{2+} on BBC250, BBC350, BBC450, and BBC550 at 298 K



and had much longer diffusive interaction time. For instance, the adsorption rates (k_2) of BBC250, BBC350, and BBC450 decreased from 0.063 to 0.008 g/(mg/h) with temperature increasing from 250 to 450 °C. The higher k_2 values signified the higher initial sorption rate in the pseudo-second-order model. Also, the initial sorption rate is related to the diffusive interaction time affected by biochar structure. The structure with more active adsorption sites would have higher k_2 values. So, the rough and monolayer structure of BBC250 with more

active adsorption sites contribute to the high initial sorption rate. These results implied that porosities and structural differences of bacteria-derived biochar could cause different diffusive interaction time so as to affect the initial cadmium sorption, which is similar with the conclusion of Abdul et al. (2017). The parameters of Elovich model (α and β) (Table S2) showed that the values of α (mg/(g/h)) were remarkably bigger than β (g/mg) for the tested bacteria-derived biochars ($p < 0.05$), which suggested that adsorption was larger than

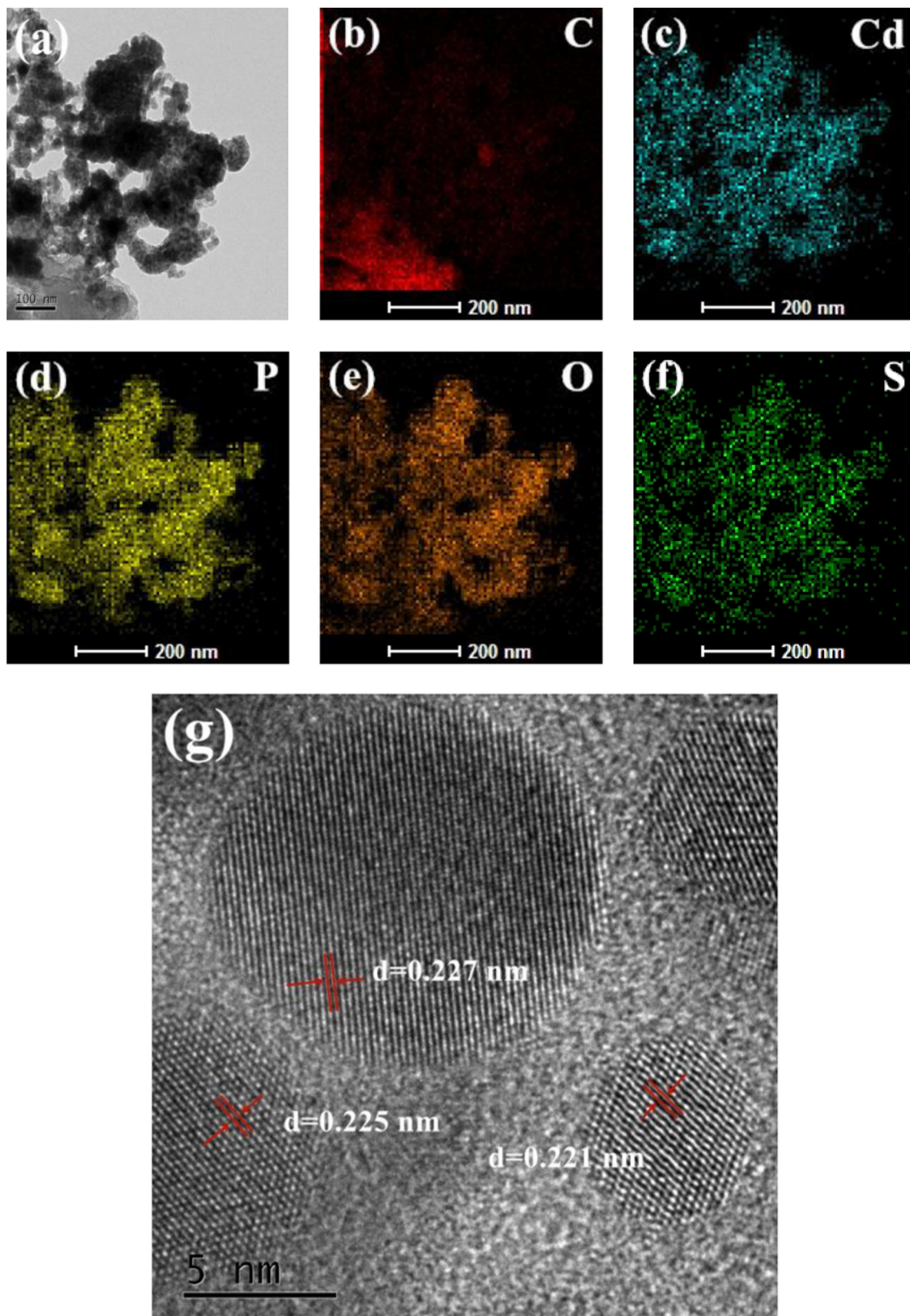


Fig. 4 **a** TEM images of BBC450 after Cd^{2+} adsorption and the corresponding EDX elemental mapping for **b** C, **c** Cd, **d** P, **e** O, **f** S, **g** HRTEM image of BBC450 after Cd^{2+} adsorption, **h** SAED pattern of BBC450 after Cd^{2+} adsorption from **g**, **i** EDS pattern of BBC450 after Cd^{2+} adsorption

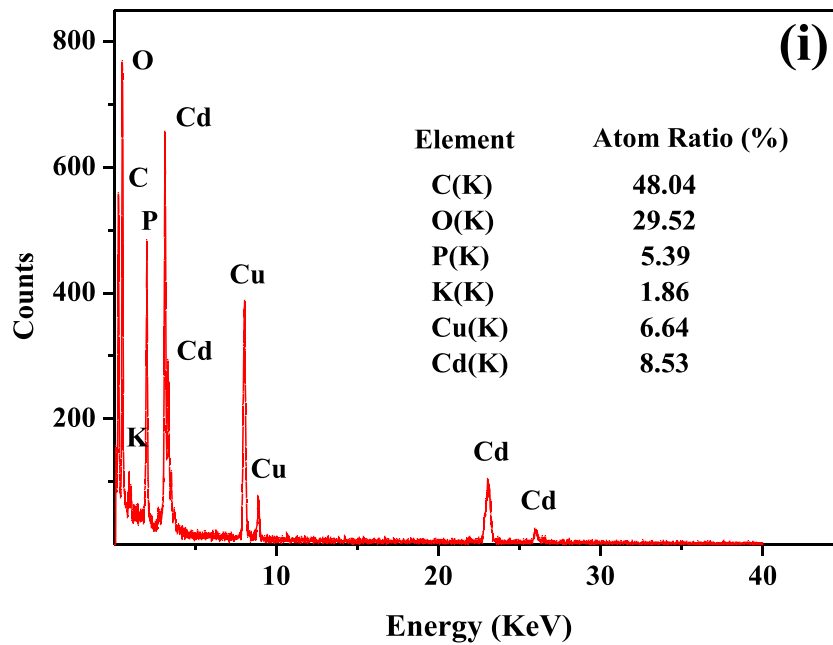
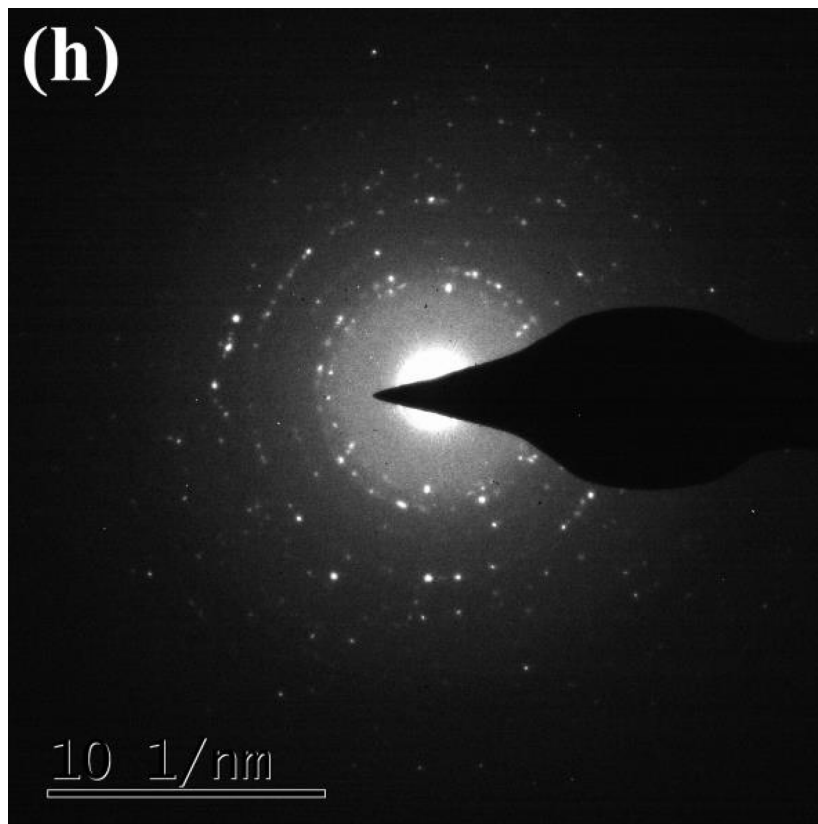


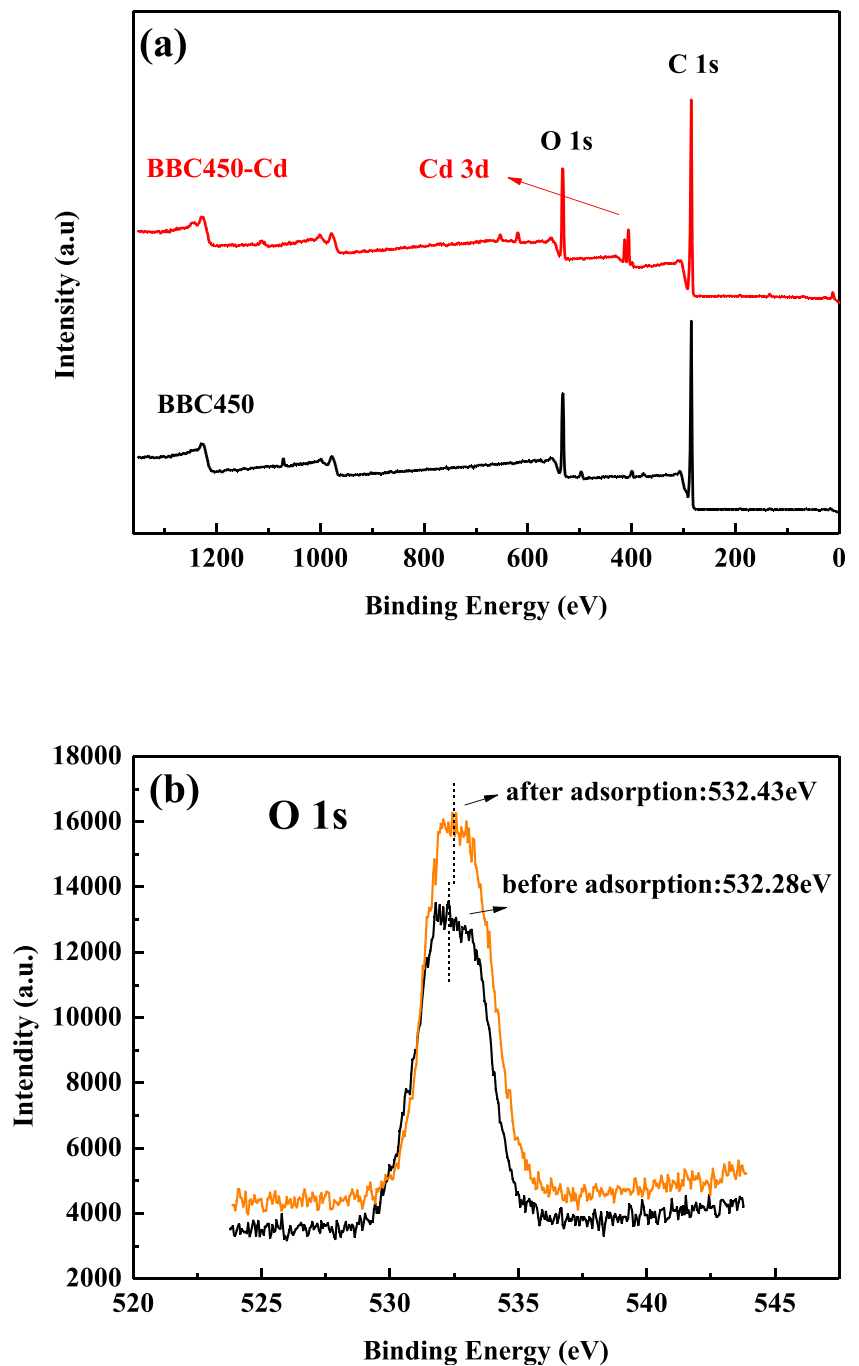
Fig. 4 (continued)

desorption during the adsorption process of Cd²⁺ onto bacteria-derived biochar (Liang et al. 2014).

The adsorption isotherms (including Langmuir and Freundlich) and their fitting parameters of Cd on biochar are

shown in Fig. 3b and Table S3, respectively. The R² of Langmuir model (the R² value of BBC250, BBC350, BBC450, and BBC550 is 0.9516, 0.9597, 0.9985, and 0.9925, respectively) was higher than Freundlich model (the

Fig. 5 XPS spectra for BBC450 before and after Cd^{2+} adsorption: **a** survey spectra, **b** O 1s, **c** P 2p, and **d** Cd 3d



R^2 value of BBC250, BBC350, BBC450, and BBC550 is 0.9145, 0.6417, 0.8942, and 0.6981, respectively), suggesting that Langmuir model could better describe the adsorption process of Cd^{2+} onto bacteria-derived biochar and the monolayer coverage sorption of Cd^{2+} and homogeneous distribution of adsorption sites on the surface of biochar (Li et al. 2016). The maximum adsorption capacities of BBC250, BBC350, BBC450, and BBC550 for Cd^{2+} calculated by Langmuir fitting were 51.52 mg/g, 38.49 mg/g, 22.21 mg/g, and 13.02 mg/g, respectively (Table S3), whereas the experimental

adsorption capacities q_e of BBC250, BBC350, BBC450, and BBC550 were 34.0 mg/g, 34.6 mg/g, 20.7 mg/g, and 12.0 mg/g, respectively (Fig. 3b). As shown in Table S1, BBC350 obviously possessed the largest surface area and total pore volume, which may be one of the reasons for its higher adsorption capacity. X-ray diffraction analysis (XRD, Fig. S6) exhibits that the (002) peak of BBC250 shifts to lower angle as compared with BBC450, meaning larger interlayer distance of BBC250 attributed to its layered structure, which lead to higher specific surface area (SSA) for BBC250 (Long et al.

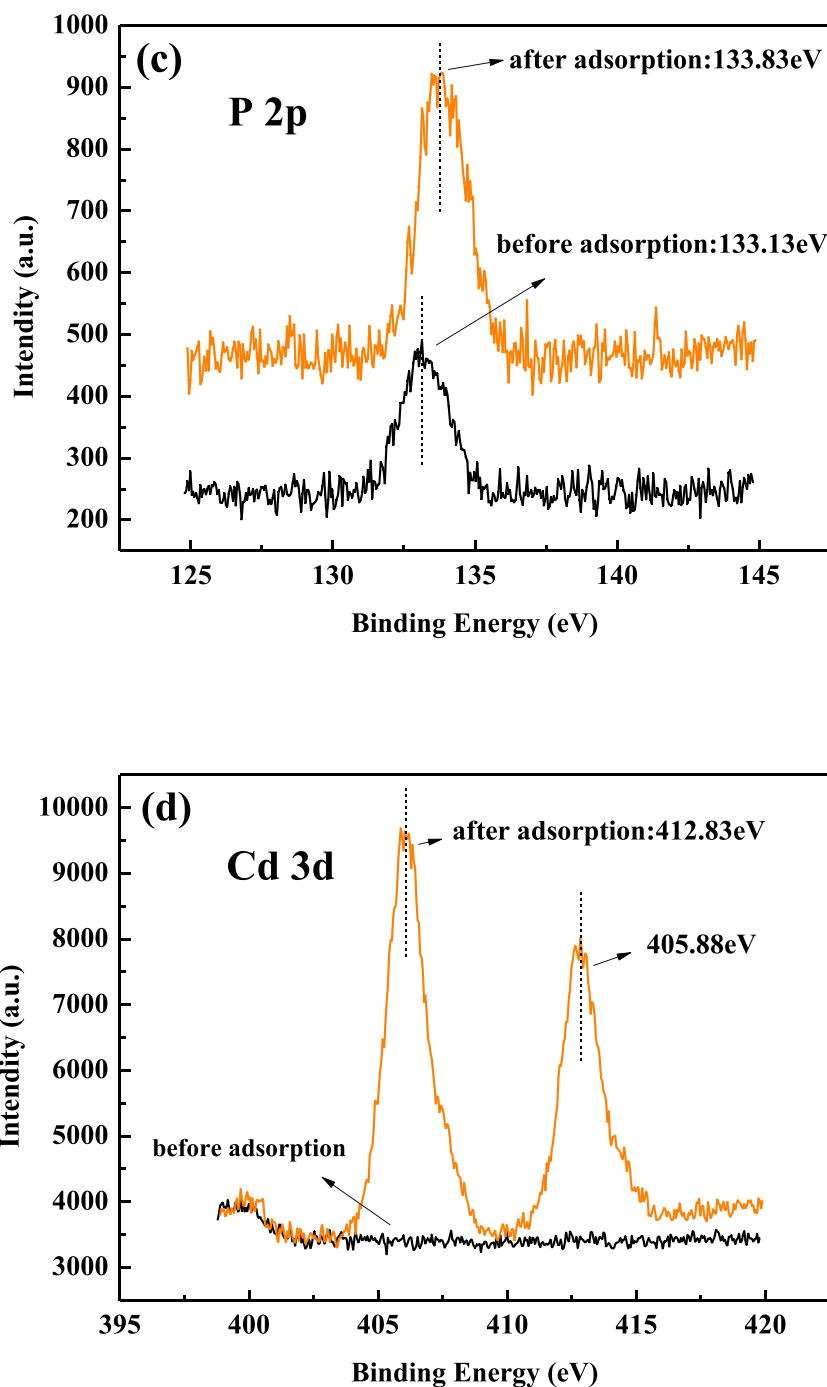


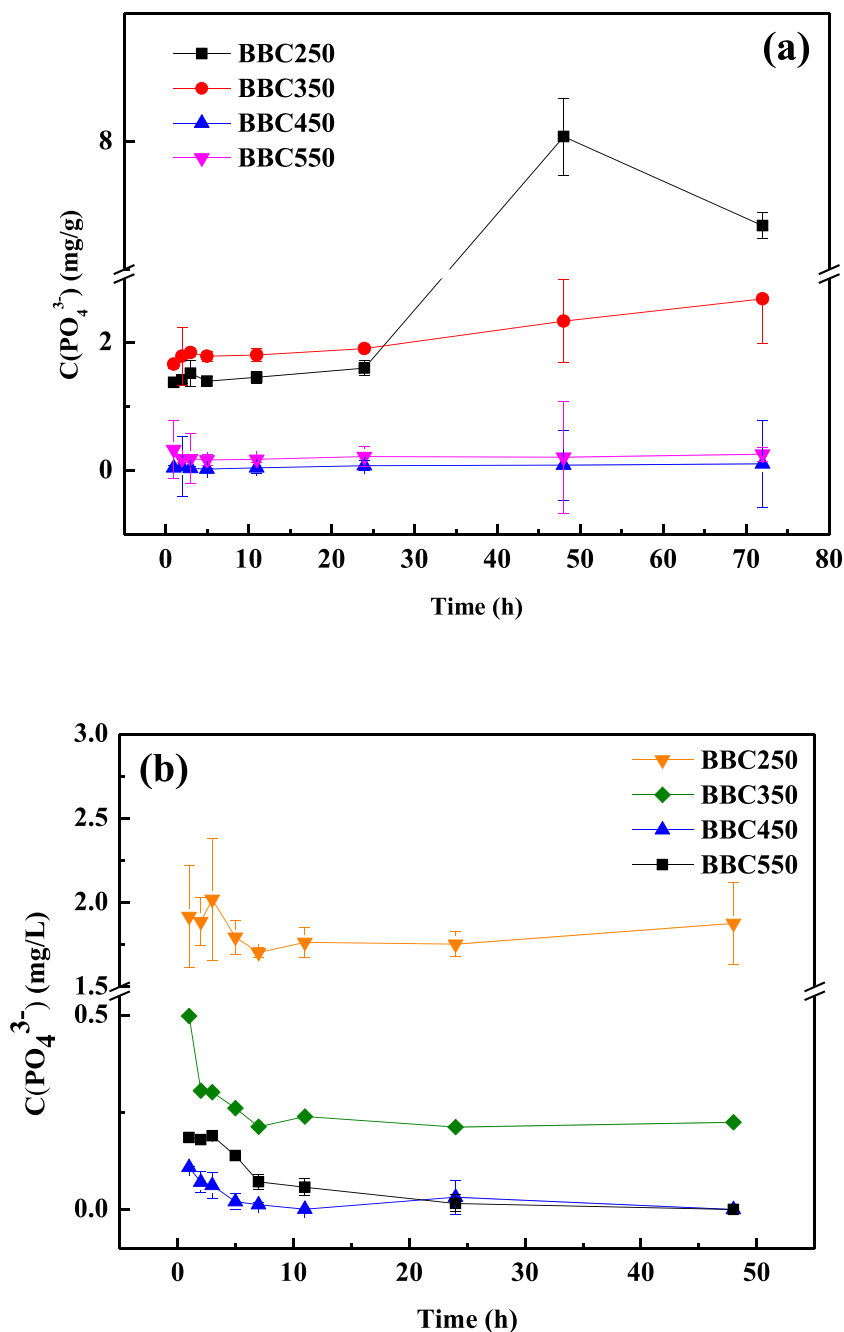
Fig. 5 (continued)

2015). The graphene-like layers may stack up and the differences of interlayer distance may be the reason for biochar prepared in low temperature has bigger SSA. Notably, the adsorption capacity of bacteria-derived biochar for Cd²⁺ decreased with an increased pyrolytic temperature from 250 to 550 °C, which might be because that the functional group C=C (1582 cm⁻¹) became stronger whereas C=O (1647 cm⁻¹) became weaker when temperature increased from 250 to 550 °C, resulting in a weaker cation-π interaction

for BBC450 and BBC550 (as the results of FTIR shown in Fig. S3) (Deng et al. 2019).

The high temperature was favored for sorption of Cd²⁺ on straw biochar because of their richer pore structure with the increase of pyrolysis temperature (Liu and Fan 2018; Gao et al. 2019); however, straw biochar can only grab Cd²⁺ on the surface. The sorption capacity of bacterial biochar for Cd²⁺ decreased as the pyrolysis temperature increased, which might be due to larger interlayer distance and rougher surface in low

Fig. 6 a Release of PO_4^{3-} from BBCX (10 mg) in 0.01 mol/L NaNO_3 solution at whole 72 h, **b** the concentrations of PO_4^{3-} in 0.01 mol/L NaNO_3 solution under the addition of 25 mg/L Cd^{2+} and 10 mg BBCX at whole 48 h. X represents 250, 350, 450, and 550, respectively



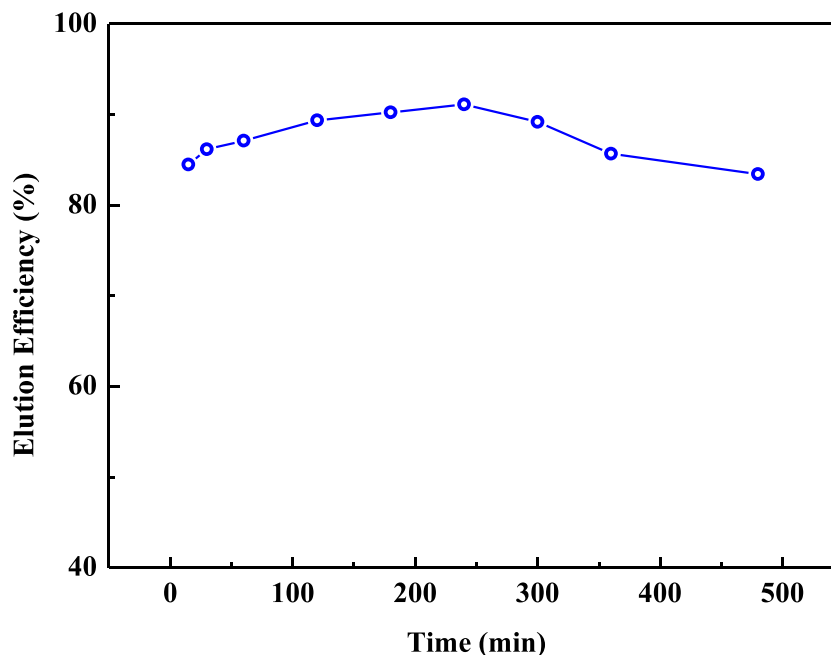
temperature biochar such as BBC250. However, the polyptychial mesoporous structure of bacterial biochar could help the precipitate contained Cd entering into the layer space and subsequently be sequestered, which was verified by SEM image (Fig. 2d) and the lattice line and diffraction ring in HRTEM image (Fig. 4g, h). More importantly, the differences presented between bacterial biochar and straw biochar are derived from their natural structure differences. Straw are mainly consisted of hollow tubular structure while bacteria are mainly composed by peptidoglycan layer. After pyrolysis, straw biochar or bacteria-derived biochar remained corresponding natural structures. Thus, the properties and

structures of bacteria-derived biochar are different with that of straw biochar, resulting in many differences described above.

Sequestration of Cd^{2+} by bacteria-derived biochar

As expected, the changes of the structural morphology and properties for BBC250, BBC350, BBC450, and BBC550 were favorable to adsorption and sequestration of Cd^{2+} . As shown in SEM images Fig. 2c, d, the surface of BBC550 was relatively uniform and smooth before adsorption of Cd^{2+} . While some visible particles (possibly precipitates and/or

Fig. 7 The leaching curve of adsorbed Cd^{2+} on BBC350 at 25 °C, where the adsorption amount of Cd^{2+} was 31.955 mg/g



minerals) appeared on the surface and inside layers of BBC550, suggesting Cd^{2+} reacted with the functional groups and/or components of biochar to form the Cd-related compounds (Zhang et al. 2015).

Compared to pre-sorption bacteria-derived biochars, many black depositional dots with distinct shape were remarkably observed on HRTEM image of Cd-loaded BBC450 (Fig. 4a). The corresponding EDS spectra of the depositional dots showed high peaks of Cd, P, and O elements (Fig. 4i), which demonstrated the sequestration of Cd^{2+} was strongly associated with P and O (Chen et al. 2018). The results were further supported by the results of TEM-mapping analysis (Fig. 4b–f). The phosphate-bridged ternary complexes, such as P–Cd and P–O–Cd, might be the key compounds responsible for effective sequestration of Cd^{2+} (Ma et al. 2015; Liu et al. 2018b; Lei et al. 2019). To obtain an insight into the detailed characteristics of flocculent sedimentary particles, HRTEM equipped with electron diffraction was carried out. BBC450 after adsorption of Cd^{2+} displayed obvious crystal and amorphous natures, where the lattice fringe spacing of observed crystal particles was approximately 0.225 nm (Fig. 4g), and the diffraction ring features were remarkable (Fig. 4h). In contrast, no lattice fringe (Fig. S3b) and corresponding diffraction ring (Fig. S3c) were observed in the control biochar (without Cd^{2+} sorption). These results suggested that Cd^{2+} adsorbed onto bacteria-derived biochar formed polycrystalline cadmium salt (Li et al. 2018), and highlighted the critical role of phosphate-bridged ternary complexes formation in the sequestration of Cd^{2+} and thereby reduced bioavailability of Cd^{2+} .

To reveal chemical components of the formed mineral particles on bacteria-derived biochar after adsorption of Cd^{2+} , the Cd-loaded BBC450 were further examined using XPS analysis. As shown in Fig. 5a, two new peaks appeared at binding

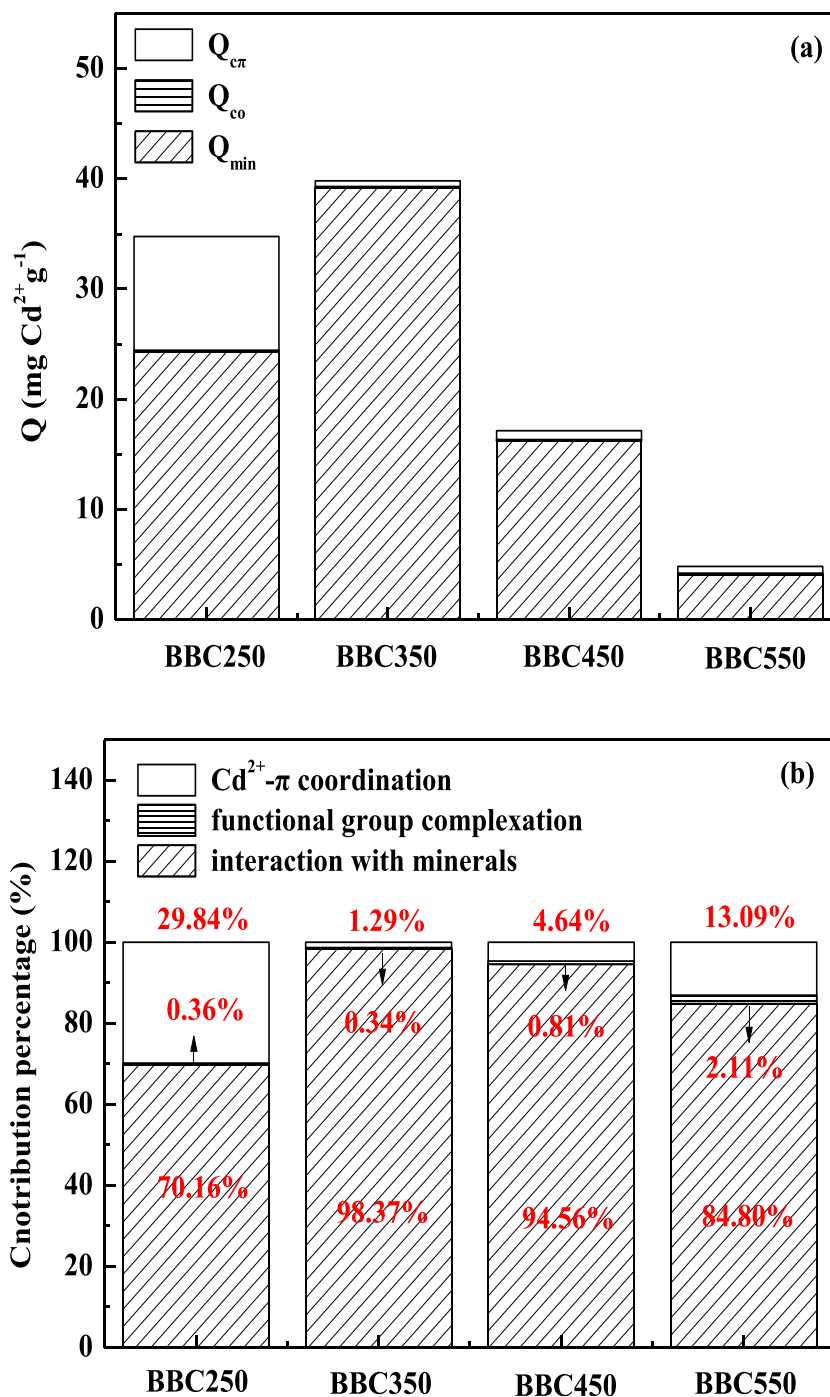
energy of 405.8 eV and 412.8 eV, indicating the precipitation of Cd mineral(s) onto the bacteria-derived biochar surface. As shown in Fig. 5c, the highest peak energy of “P 2p” for the BBC450 before Cd adsorption was 133.13 eV, whereas that of “P 2p” for BBC450 after Cd adsorption increased to 133.83 eV. This observation indicated that element P might bond with Cd and O atoms during the adsorption process of Cd^{2+} , which was also supported by the higher binding energy of Cd 3d and O 1s (Fig. 5b, d). The results in this study indicated the formation of phosphate-bridged ternary complexes (Zhu et al. 2014; Liu et al. 2018b) probably the cadmium orthophosphate, despite previous studies also reported the other three types of Cd minerals, cadmium carbonate, and cadmium chloride (Zhang et al. 2015) were identified in the post-sorption biochar.

Notably, after Cd^{2+} adsorption, the peaks at 292.9 eV and 295.7 eV disappeared in C 1s spectrum, referring to K 2p_{3/2} and K 2p_{1/2}, respectively (Fig. S4), which suggested that K^{+} was released from BBC450 surface (Chen et al. 2018), implying that the ion exchanges occurred between Cd and surface ions of biochar.

Phosphorus release from biochar favoring sequestration of Cd^{2+}

The aforementioned results illuminated that phosphorus played an important role in Cd^{2+} sequestration, the phosphorus (here referring to PO_4^{3-}) release from biochar was thus investigated. As shown in Fig. 6a, BBC250 and BBC350 released more phosphorus than that of BBC450 and BBC550 (i.e., 8.0 and 2.3 mg/g for BBC250 and BBC350 vs. 0.085 and 0.021 mg/g for BBC450 and BBC550,

Fig. 8 **a** The contribution capacities for Cd^{2+} sorption on bacteria-derived biochars by interaction with minerals (Q_{min}), functional groups complexation (Q_{co}), and Cd^{2+} - π coordination (Q_{cr}). **b** The corresponding contribution percentage of the Cd^{2+} sorption mechanisms described in **a**



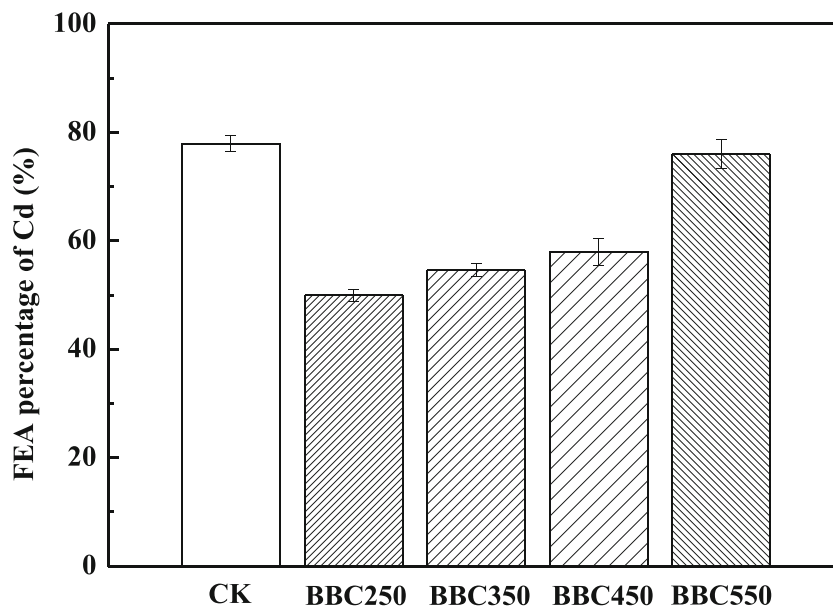
respectively). This result might be ascribed to the decrease of the soluble phosphorus in the biochar produced at more higher pyrolysis temperatures (> 450 °C) because amorphous P-Ca-Mg could crystallize to form less soluble phases at higher temperatures (Cao and Harris 2010). When Cd^{2+} was added, the concentration of PO_4^{3-} in supernatant decreased, suggesting that the released phosphorus (e.g., PO_4^{3-}) favored the binding with Cd^{2+} and even finally formed polycrystalline particles (Xu et al. 2013; Zhao et al. 2016). In a word, biochar

could be considered as a kind of soil additive that could sequestration cadmium ions coupling with slow phosphorus release in term of fertilizers.

The evaluation for sequestration of Cd^{2+} by bacteria-derived biochar

In order to evaluate the sequestration efficiency of Cd^{2+} by bacteria-derived biochar, the leaching experiment of Cd^{2+}

Fig. 9 The corresponding percentage (%) of FEA Cd in tested paddy soils under the addition of BBC250, BBC350, BBC450, and BBC550 as the ratio of 1% (w/w), respectively. CK represents no addition of bacteria-derived biochar



from Cd-loaded BBC350 was carried out. As shown in Fig. 7, the adsorption amount of Cd²⁺ by BBC350 achieved 32.0 mg/g in the sorption stage; however, when the BBC350 adsorbed Cd²⁺ was added into HNO₃ solution (0.1 mol/L), absorbed Cd²⁺ was released approximately 90% of the adsorption amount of Cd²⁺ on BBC350 during whole 240 min. The residual Cd amount on BBC350 was 3.2 mg/g, and the residual Cd was sequestered in the pores of BBC350 in form of insoluble polycrystalline and/or amorphous phosphate-bridged ternary complex.

Contribution of Cd²⁺ sorption mechanisms

The contribution of the interaction with minerals (Q_{min}), functional groups complexation (Q_{co}), and Cd²⁺- π coordination ($Q_{c\pi}$) to the total Cd²⁺ sorption (Q_t) on biochars is shown in Fig. 8. The contribution of Cd²⁺- π coordination increased with increasing pyrolysis temperature from 350 to 550 °C, while the contribution of interaction with minerals presented the reverse trend. For example, the $Q_{c\pi}/Q_t$ value of BBC350 was 1.3%; however, the $Q_{c\pi}/Q_t$ value of BBC550 increased to 13.1%. Conversely, the Q_{min}/Q_t value of BBC350 was 98.4%, but the Q_{min}/Q_t value of BBC550 was only 84.8%. This phenomenon might be mainly because the pyrolysis temperature affected the reserved amount of oxygen containing functional groups and aromaticity difference of biochars (Cui et al. 2016). These results were also consistent with the analysis of the FIRT spectrum (Fig. S2). The Q_{min} values of bacteria-derived biochars accounted for 70.2–98.4% of their Q_t values, indicating that the interaction between Cd²⁺ and minerals is a dominant mechanism of Cd²⁺ sorption on bacteria-derived biochars.

FEA-Cd in paddy soil

As shown in Fig. 9, after 10 days, almost all amendments of BBC250, BBC350, BBC450, and BBC550 decreased significantly the content of FEA-Cd in the tested soils ($p < 0.05$). For instance, the lowest FEA-Cd (49.96%) was achieved by BBC250 amendment compared to the other bacteria-derived biochars. This might be because BBC250 had higher sorption capacity (Fig. 3b). Nevertheless, the addition of bacteria-derived biochars could reduce Cd bioavailability in the tested paddy soils, which would be potentially applied to immobilize Cd in the Cd-contaminated soil.

Conclusions

The results of this study showed that the polyptychial mesoporous graphite-like properties of BBC350 promoted the adsorption and sequestration of Cd²⁺ indicated by the images of lattice line and diffraction ring. The interaction with minerals (including surface precipitation with phosphorus and ion exchange) played a dominant role by forming insoluble cadmium salt composed by polycrystalline and/or amorphous phosphate-bridged ternary complex during the process of Cd²⁺ sorption and sequestration. The saturated sorption capacities of bacteria-derived biochars for Cd²⁺ were 12–34 mg/g in simulated soil water phase. Moreover, bacteria-derived biochar amendments (1%, w/w) reduced the fractions easily absorbed by plants for Cd in the test paddy soils by 1.9–26% during 10 days. Therefore, bacteria-derived biochar would be promisingly applied in remediation of soils contaminated by heavy metals.

Funding information This work was supported by the National Natural Science Foundation of China (21577118 and 41701580), National Key Research and Development Plan of China (2016YFD0800700), China Postdoctoral Science Foundation Funded Project (2016M590749, 2017T100605, and 2018M642992), the Natural Science Foundation of Hunan Province (2016JJ1024), Key Research and Development Plan of Hunan Province (2018SK2045 and 2018SK2042) and Collaborative Innovation Center of New Chemical Technologies for Environmental Benignity and Efficient Resource Utilization as well as Key Laboratory of Soil Environment and Pollution Remediation, Institute of Soil Science, Chinese Academy of Sciences (SER2017-05).

References

- Abdul G, Zhu X, Chen B (2017) Structural characteristics of biochar-graphene nanosheet composites and their adsorption performance for phthalic acid esters. *Chem Eng J* 319:9–20
- Ahmad M, Rajapaksha AU, Lim JE, Zhang M, Bolan N, Mohan D, Vithanage M, Lee SS, Ok YS (2014) Biochar as a sorbent for contaminant management in soil and water: a review. *Chemosphere* 99:19–33
- Cao X, Harris W (2010) Properties of dairy-manure-derived biochar pertinent to its potential use in remediation. *Bioresour Technol* 101:5222–5228
- Chen L, Shi G, Shen J, Peng B, Zhang B, Wang Y, Bian F, Wang J, Li D, Qian Z, Xu G, Liu G, Zeng J, Zhang L, Yang Y, Zhou G, Wu M, Jin W, Li J, Fang H (2017) Ion sieving in graphene oxide membranes via cationic control of interlayer spacing. *Nature* 550:380–383
- Chen Z, Liu T, Tang J, Zheng Z, Wang H, Shao Q, Chen G, Li Z, Chen Y, Zhu J, Feng T (2018) Characteristics and mechanisms of cadmium adsorption from aqueous solution using lotus seedpod-derived biochar at two pyrolytic temperatures. *Environ Sci Pollut Res* 25:11854–11866
- Chien SH, Clayton WR (1980) Application of Elovich equation to the kinetics of phosphate release and sorption in soils 1. *Soil Sci Soc Am J* 44:265–268
- Cui X, Fang S, Yao Y, Li T, Ni Q, Yang X, He Z (2016) Potential mechanisms of cadmium removal from aqueous solution by *Canna indica* derived biochar. *Sci Total Environ* 562:517–525
- Deng Y, Huang S, Laird DA, Wang X, Meng Z (2019) Adsorption behaviour and mechanisms of cadmium and nickel on rice straw biochars in single- and binary-metal systems. *Chemosphere* 218:308–318
- Gao LY, Deng JH, Huang GF, Li K, Cai KZ, Liu Y, Huang F (2019) Relative distribution of Cd²⁺ adsorption mechanisms on biochars derived from rice straw and sewage sludge. *Bioresour Technol* 272:114–122
- Guo Z, Zhang X, Kang Y, Zhang J (2017) Biomass-derived carbon sorbents for cd(II) removal: activation and adsorption mechanism. *ACS Sustain Chem Eng* 5:4103–4109
- Harvey OR, Herbert BE, Rhue RD, Kuo LJ (2011) Metal interactions at the biochar-water interface: energetics and structure-sorption relationships elucidated by flow adsorption microcalorimetry. *Environ Sci Technol* 45:5550–5556
- Jiang Y, Yan J, Wu X, Shan D, Zhou Q, Jiang L, Yang D, Fan Z (2016) Facile synthesis of carbon nanofibers-bridged porous carbon nanosheets for high-performance supercapacitors. *J Power Sources* 307:190–198
- Klupfel L, Keiluweit M, Kleber M, Sander M (2014) Redox properties of plant biomass-derived black carbon (biochar). *Environ Sci Technol* 48:5601–5611
- Lei S, Shi Y, Qiu Y, Che L, Xue C (2019) Performance and mechanisms of emerging animal-derived biochars for immobilization of heavy metals. *Sci Total Environ* 646:1281–1289
- Li F, Li D, Li X, Liao J, Li S, Yang J, Yang Y, Tang J, Liu N (2016) Microorganism-derived carbon microspheres for uranium removal from aqueous solution. *Chem Eng J* 284:630–639
- Li F, Wang W, Li C, Zhu R, Ge F, Zheng Y, Tang Y (2018) Self-mediated pH changes in culture medium affecting biosorption and biomineralization of Cd²⁺ by *Bacillus cereus* Cd01. *J Hazard Mater* 358:178–186
- Liang Y, Cao X, Zhao L, Xu X, Harris W (2014) Phosphorus release from dairy manure, the manure-derived biochar, and their amended soil: effects of phosphorus nature and soil property. *J Environ Qual* 43:1504–1509
- Liu J, Liu W, Ji S, Wan Y, Yin H, Zhou Y (2014) Facile Synthesis of Carbon-Encapsulated Li₄Ti₅O₁₂@C Hollow Microspheres as Superior Anode Materials for Li-Ion Batteries. *Eur J Inorg Chem* 12:2073–2079
- Liu L, Fan S (2018) Removal of cadmium in aqueous solution using wheat straw biochar: effect of minerals and mechanism. *Environ Sci Pollut Res* 25:8688–8700
- Liu L, Li W, Song W, Guo M (2018a) Remediation techniques for heavy metal-contaminated soils: principles and applicability. *Sci Total Environ* 633:206–219
- Liu J, Zhu R, Liang X, Ma L, Lin X, Zhu J, He H, Parker SC, Molinari M (2018b) Synergistic adsorption of cd(II) with sulfate/phosphate on ferrihydrite: an in situ ATR-FTIR/2D-COS study. *Chem Geol* 477:12–21
- Long C, Chen X, Jiang L, Zhi L, Fan Z (2015) Porous layer-stacking carbon derived from in-built template in biomass for high volumetric performance supercapacitors. *Nano Energy* 12:141–151
- Luo M, Lin H, Li B, Dong Y, He Y, Wang L (2018) A novel modification of lignin on corn-cob-based biochar to enhance removal of cadmium from water. *Bioresour Technol* 259:312–318
- Ma L, Zhu J, Xi Y, Zhu R, He H, Liang X, Ayoko GA (2015) Simultaneous adsorption of cd (II) and phosphate on Al₁₃ pillared montmorillonite. *RSC Adv* 5:77227–77234
- Matias VRF, Beveridge TJ (2005) Cryo-electron microscopy reveals native polymeric cell wall structure in *Bacillus subtilis* 168 and the existence of a periplasmic space. *Mol Microbiol* 56:240–251
- Mendonça FG, Cunha ITD, Soares RR, Tristao JC, Lago RM (2017) Tuning the surface properties of biochar by thermal treatment. *Bioresour Technol* 246:28–33
- MEP (2016) The Ministry of Land and resources Report on the national soil contamination survey. <http://www.gov.cn/foot/2014-2004/2017/content2661768.htm> (in Chinese). Accessed 29 Sept 2016
- O'Connor D, Peng T, Zhang J, Tsang DCW, Alessi DS, Shen Z, Bolan NS, Hou D (2018) Biochar application for the remediation of heavy metal polluted land: a review of in situ field trials. *Sci Total Environ* 619-620:815–826
- Pal D, Maiti SK (2019) Abatement of cadmium (cd) contamination in sediment using tea waste biochar through meso-microcosm study. *J Clean Prod* 212:986–996
- Peng JF, Song YH, Yuan P, Cui XY, Qiu GL (2009) The remediation of heavy metals contaminated sediment. *J Hazard Mater* 161:633–640
- Qiao JT, Liu TX, Wang XQ, Li FB, Lv YH, Cui JH, Zeng XD, Yuan YZ, Liu CP (2018) Simultaneous alleviation of cadmium and arsenic accumulation in rice by applying zero-valent iron and biochar to contaminated paddy soils. *Chemosphere* 195:260–271
- Tessier A, Campbell PGC, Bisson M (1979) Sequential extraction procedure for the speciation of particulate trace metals. *Anal Chem*:544e551
- Walker DJ, Clemente R, Roig A, Bernal MP (2003) The effects of soil amendments on heavy metal bioavailability in two contaminated Mediterranean soils. *Environ Pollut* 122:303–312

- Wang RZ, Huang DL, Liu YG, Zhang C, Lai C, Zeng GM, Cheng M, Gong XM, Wan J, Luo H (2018) Investigating the adsorption behavior and the relative distribution of Cd^{2+} sorption mechanisms on biochars by different feedstock. *Bioresour Technol* 261:265–271
- Xiao X, Chen B, Chen Z, Zhu L, Schnoor JL (2018) Insight into multiple and multilevel structures of biochars and their potential environmental applications: a critical review. *Environ Sci Technol* 52:5027–5047
- Xu X, Cao X, Zhao L, Wang H, Yu H, Gao B (2013) Removal of Cu, Zn, and Cd from aqueous solutions by the dairy manure-derived biochar. *Environ Sci Pollut Res* 20:358–368
- Yang H, Yan R, Chen H, Lee DH, Zheng C (2007) Characteristics of hemicellulose, cellulose and lignin pyrolysis. *Fuel* 86:1781–1788
- Yoo S, Chung CC, Kelley SS, Park S (2018) Graphitization behavior of loblolly pine wood investigated by in situ high temperature X-ray diffraction. *ACS Sustain Chem Eng* 6:9113–9119
- Yu WS (2016) Agricultural and Agri-environment policy and sustainable agricultural development in China. IFRO report 247, University of Copenhagen, pp 6–15. https://www.researchgate.net/publication/301635451_Agricultural_and_agrienvironment_policy_and_sustainable_agricultural_development_in_China
- Yu H, Zou W, Chen J, Chen H, Yu Z, Huang J, Tang H, Wei X, Gao B (2018) Biochar amendment improves crop production in problem soils: a review. *J Environ Manag* 232:8–21
- Yuan J, Xu S, Zeng HY, Cao X, Dan Pan A, Xiao GF, Ding PX (2018) Hydrogen peroxide biosensor based on chitosan/2D layered double hydroxide composite for the determination of H_2O_2 . *Bioelectrochemistry* 123:94–102
- Zhang F, Wang X, Yin D, Peng B, Tan C, Liu Y, Tan X, Wu S (2015) Efficiency and mechanisms of Cd removal from aqueous solution by biochar derived from water hyacinth (*Eichornia crassipes*). *J Environ Manag* 153:68–73
- Zhao L, Cao X, Zheng W, Scott JW, Sharma BK, Chen X (2016) Coprolysis of biomass with phosphate fertilizers to improve biochar carbon retention, slow nutrient release, and stabilize heavy metals in soil. *ACS Sustain Chem Eng* 4:1630–1636
- Zhu R, Li M, Ge F, Xu Y, Zhu J, He H (2014) Co-sorption of Cd and phosphate on the surface of a synthetic hydroxyiron-montmorillonite complex. *Clay Clay Miner* 62:79–88

Publisher's note Springer Nature remains neutral with regard to jurisdictional claims in published maps and institutional affiliations.